NASA CONTRACTOR REPORT

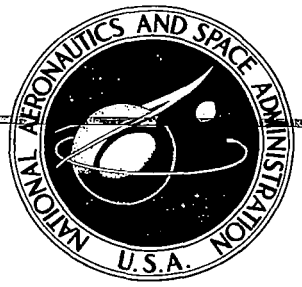

NASA CR-2

NASA CR-2641

INVESTIGATION OF THERMAL FATIGUE IN FIBER COMPOSITE MATERIALS

Abdel A. Fahmy and Thomas G. Cunningham

Prepared by
NORTH CAROLINA STATE UNIVERSITY
Raleigh, N.C.
for Langley Research Center

NATIONAL AERONAUTICS AND SPACE ADMINISTRATION • WASHINGTON, D. C. • JULY 1976

1. Report No.	2. Government Accession No.	3. Recipient's Catalog No.
NASA CR-2641		

4. Title and Subtitle	5. Report Date
INVESTIGATION OF THERMAL FATIGUE IN FIBER COMPOSITE MATERIALS	July 1976
	6. Performing Organization Code

7. Author(s)	8. Performing Organization Report No.
Abdel A. Fahmy and Thomas G. Cunningham	
	10. Work Unit No. 505-02-31-01

9. Performing Organization Name and Address	11. Contract or Grant No.
North Carolina State University Department of Materials Engineering Raleigh, North Carolina	NGR 34-002-180
	13. Type of Report and Period Covered
12. Sponsoring Agency Name and Address	Contractor Report
National Aeronautics and Space Administration Washington, D.C. 20546	14. Sponsoring Agency Code

15. Supplementary Notes

Abstract by NASA Grant Monitor, L. A. Imig

Final Report

16. Abstract

Graphite-epoxy laminates were thermally cycled to determine the effects of thermal cycles on tensile properties and thermal expansion coefficients of the laminates. Three 12-ply laminate configurations, (unidirectional, $[[\pm 45_3]_2]_T$, and $[0/30/60/90/-60/-30]_S$) were subjected to up to 5000 thermal cycles. The cumulative effect of the thermal cycles was determined by destructive inspection (electron micrographs and tensile tests) of samples after progressively larger numbers of cycles.

After thermal cycling, the materials' tensile strengths, moduli, and thermal expansion coefficients were significantly lower than for the materials as fabricated. Most of the degradation of properties occurred after only a few cycles.

The property degradation was attributed primarily to the progressive development of matrix cracks whose locations depended upon the layup orientation of the laminate.

17. Key Words (Suggested by Author(s))	18. Distribution Statement
composite materials graphite-epoxy thermal cycling mechanical properties	Unclassified, Unlimited Subject Category 24

19. Security Classif. (of this report)	20. Security Classif. (of this page)	21. No. of Pages	22. Price*
Unclassified	Unclassified	60	$4.25

*For sale by the National Technical Information Service, Springfield, Virginia 22161

TABLE OF CONTENTS

LIST OF TABLES

LIST OF FIGURES

INTRODUCTION

Only recently have graphite fibers been used to reinforce plastics for ablative and structural composite applications. The potential of graphite as a high strength, high modulus reinforcing material became evident when graphite whiskers were produced with a tensile strength of 20×10^9 N/m^2 and Young's modulus values higher than 70×10^{10} N/m^2 (1).

Graphite fiber-reinforced composites have been widely used since 1959 in ablative applications. It was not until six years later, in 1965, with the introduction of high modulus, high strength graphite fiber that graphite-fiber composites were seriously considered for structural application. Since that time, development and evaluation of these composites have progressed at an increasingly rapid rate (1).

This investigation was initiated to further evaluate the graphite-epoxy composite material under conditions of thermal fatigue and to make possible the production of better fiber composites through a better understanding of the influence of fiber orientation and lamination sequence on their thermal fatigue performance.

LITERATURE SURVEY

Mechanical Properties

To evaluate the effect of thermal cycling on the elastic and strength properties of a laminated composite, the elastic properties and the thermal expansion properties of a unidirectional composite of the same material and proportions must be known. In addition, the configurations of the laminate and structural defects must be known.

In order to study a laminated composite, it is necessary to consider a unidirectional material composed of a parallel set of cylindrical fibers embedded in a homogeneous matrix material. The elastic constants of this material are evaluated as a function of the average stress and strain imposed on the material. In the most general case, this material may be orthotropic having nine independent elastic constants. If a material such as continuous graphite fiber is used, the individual layers have a multiplicity of filaments through the thickness. A cross section, perpendicular to the fiber, of the material would show a random distribution of fiber cross-sections. This would indicate that the transverse plane would be a plane of isotropy and that the composite would be treated as a transversely isotropic composite with only five independent elastic constants. For an existing material, the five independent constants can be evaluated by direct experimental methods. Hill (2) developed structural relations that simplified the problems associated with determining these moduli. He was able to show the interrelation of the axial Young's modulus, Poisson's ratio, and the plane strain

bulk modulus. By knowing these three, the other two effective composite properties can be determined.

The experimental data generated for fiber composites are usually directed toward their ultimate use in the form of shells or laminated plate. In this case only four of the five independent elastic constants are generally considered. These are the axial and transverse Young's modulus, Poisson's ratio, and the axial shear modulus.

Once the effective elastic constants of the unidirectional fiber composite are known, the material may be viewed as a homogeneous orthotropic material. Then for laminates formed from layers of unidirectional composites, it is reasonable to treat each layer as an orthotropic continuum, and to study the laminate using layered plate theory. This theory is in widespread use for all types of composites, and has been shown to be a suitable starting point for structural analysis (3). The constants in this relationship are evaluated by using the stress-strain relationship for individual plys or layers and the Kirchoff Hypothesis for thin plates (4).

Thermal Properties

Evaluation of the response of composite materials to temperature changes is important not only for applications involving such temperature changes in service, but also for fabrication consideration such as the choice of the cure temperature for fiber reinforced plastics. Even though much work has been done on elastic behavior of unidirectional and laminated composites (5), little has been

reported on their thermal behavior. This behavior may influence dimensional stability, strength, and mechanical compatibility in structural assemblies.

The thermal expansion coefficient of an unidirectional composite in the longitudinal direction can be predicted from the following formula which is based on equilibrium and compatibility considerations (4).

$$\alpha_L = (\alpha_m V_m E_m + \alpha_f V_f E_f)/(V_m E_m + V_f E_f)$$

where α_m and α_f are the expansion coefficients of the matrix and fiber, respectively, E_m and E_f are their Young's moduli, and V_m and V_f are their volume fractions. This shows that the longitudinal coefficient is a weighted average of the volume fraction and tensile modulus of the fiber and matrix. This would indicate that the longitudinal coefficient of the composite would be almost the same as that of the graphite in a graphite-epoxy system since the tensile modulus of the fiber is two to three orders of magnitude greater than that of the matrix. In the transverse direction, the constituents play more proportionate roles. However, its calculation involves the transverse properties of the fibers, which at the present time are not known with certainty (6).

Even though it is possible to calculate the thermal coefficients of an unidirectional fiber composite assuming purely elastic behavior, the transverse coefficient is so sensitive to the actual shape and distribution of the fibers that the calculated values are not very reliable. Thus, in calculating the in-plane thermal expansion coefficient in any direction of a laminated panel, it is advisable to obtain α_L and α_T experimentally.

A simple rule of mixtures should give the thermal expansion coefficients of a composite material provided that there is no plane interaction. However, differences in thermal expansivities of individual phases give rise to a state of microstresses between phases (6). Fahmy et al (6) demonstrated the existence of these thermally induced stresses in glass-metal composites by the use of x-rays.

In laminated composite materials, stress states are generally set up in each layer when the temperature changes since the layer is not free to expand by an amount α_L in the longitudinal and α_t in the transverse directions. The layers expand by α_1 and α_2 of the composite in the direction of the 1 and 2 axis as illustrated in Figure 1.

Doner and Novak (7) showed that translamina cracks found in graphite-epoxy laminates were the result of thermal stresses induced as the composite cooled from a relatively strain-free curing temperature to room temperature. Further work by Spain (8) indicates that the severity of cracking is directly related to the amount of resin shrinkage during curing. Spain (8) also found that even if the composites were fabricated in a stress free state, that subsequent thermal cycling usually produced microcracks.

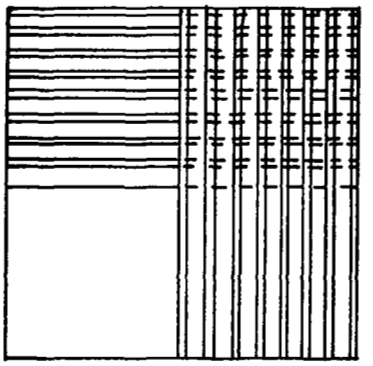

No Expansion

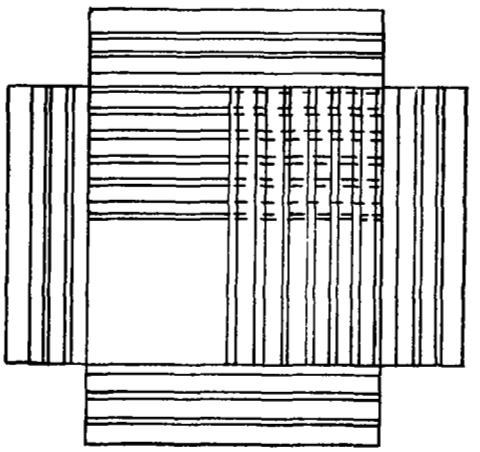

Free Expansion

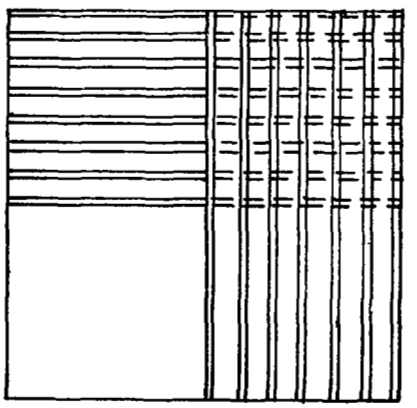

Constrained Expansion

Figure 1. Thermal Expansion of Constrained and Non-Constrained Composite Materials

THEORETICAL CONSIDERATION

Modulus of Elasticity

For a single ply fiber composite, the modulus of elasticity, E, when the uniaxial tensile axis is along the fiber direction is given by the equation:

$$E_L = E_f V_f + E_m(1-V_f) \tag{1}$$

where: E_L = longitudinal modulus

E_f = fiber modulus

E_m = matrix modulus

V_f = volume fraction fiber

$(1-V_f)$ = volume fraction matrix

This is obtained from the stress equations

$$\sigma_c A_c = \sigma_m A_m + \sigma_f A_f \tag{2}$$

$$\sigma_c = \sigma_m V_m + \sigma_f V_f \tag{3}$$

where A represents area, V represents volume fraction, and σ_c, σ_m, σ_f represent stress in the composite, matrix and fiber. Since no slippage is allowed at the interface, the strain experienced by the composite is equal to the fiber strain and also the matrix strain.

$$\varepsilon_c = \varepsilon_m = \varepsilon_f \tag{4}$$

where ε_c is the composite strain, ε_m is the matrix strain, and ε_f is the fiber strain.

Rewriting equation 3:

$$\sigma_c A = \sigma_f \left[A_f + \frac{E_m}{E_f} A_m \right] \tag{5}$$

$$E_L = E_f \frac{A_f}{A} + E_m \frac{A_m}{A} \tag{6}$$

$$E_L = E_f V_f + E_m (1 - V_f) \tag{1}$$

When the unidirectional tensile axis is normal to the fiber direction, E is given by:

$$E_T = \frac{E_m E_f}{E_f (1 - V_f) + E_m V_f} \tag{7}$$

This equation is based on simplifying considerations. The actual equation is obtained by the simple case where:

$$\varepsilon_{Tm} = \frac{\sigma_{Tm}}{E_m} - \nu_m \frac{\sigma_{Lm}}{E_m} \tag{8}$$

$$\varepsilon_{Lm} = \frac{\sigma_{Lm}}{E_m} - \nu_m \frac{\sigma_{Tm}}{E_m} \tag{9}$$

$$\varepsilon_{Tf} = \frac{\sigma_{Tf}}{E_f} - \nu_f \frac{\sigma_{Lf}}{E_f} \tag{10}$$

$$\varepsilon_{Lf} = \frac{\sigma_{Lf}}{E_f} - \nu_f \frac{\sigma_{Tf}}{E_f} \tag{11}$$

where:

ε_{Tm} = transverse strain in the matrix

ε_{Lm} = longitudinal strain in the matrix

ε_{Tf} = transverse strain in the fiber

ε_{Lf} = longitudinal strain in fiber

ν_m = Poisson's ratio (matrix)

ν_f = Poisson's ratio (fiber)

which are fiber and matrix strains in the longitudinal (L) and transverse (T) directions. Compatibility conditions require:

$$\varepsilon_{Lm} = \varepsilon_{Lf} \tag{12}$$

and equilibrium conditions dictate that:

$$\sigma_{Tm} = \sigma_{Tf} = \sigma_T \tag{13}$$

$$\sigma_{Lm}A_m + \sigma_{Lf}A_f = 0 \tag{14}$$

If the resultant strain in the T direction is ε_T,

$$\varepsilon_T A = \varepsilon_{Tm}A_m + \varepsilon_{Tf}A_f \tag{15}$$

Solving for σ_{Lm}

$$\sigma_{Lm} = \frac{\nu_m\sigma_{Tm} - \left(\frac{E_m}{E_f}\nu_f\right)\left(\sigma_{Tf}\right)}{1 + \frac{E_m}{E_f}\frac{A_m}{E_f}} \tag{16}$$

$$\sigma_{Lm} = A_f\left(\frac{E_f\nu_m - E_m\nu_f}{E_fA_f + E_mA_m}\right)\sigma_T \tag{17}$$

Solving for $\varepsilon_T A$

$$\varepsilon_T A = \left[\frac{A_m}{E_m} + \frac{A_f}{E_f}\right]\sigma_T - A_m\sigma_{Lm}\left[\frac{\nu_m}{E_m} - \frac{\nu_f}{E_f}\right] \tag{18}$$

Substituting for σ_{Lm}

$$\frac{A_f}{A} = V \quad \frac{A_m}{A} \quad (1-V)$$

then

$$\frac{\varepsilon_T}{\sigma_T} = \frac{1}{E_m E_f}\left[E_f(1-V) + E_m V\right] - \frac{V(1-V)(\nu_m E_f - \nu_f E_m)^2}{E_m E_f[VE_f + (1-V)E_m]} \qquad (19)$$

$$\frac{\varepsilon_T}{\sigma_T} = \frac{1}{E_T}$$

$$E_T = \frac{E_m E_f[VE_f + (1-V)E_m]}{[E_f(1-V) + E_m V][E_f V + E_m(1-V)] - V(1-V)[\nu_m E_f - \nu_f E_m]^2} \qquad (20)$$

If $\nu_m \nu_f$, $\nu_f{}^2$, and $\nu_m{}^2 \ll 1$

then:

$$E_T = \frac{E_m E_f}{E_f(1-V) + E_m V} \qquad (7)$$

If then a value of the shear modulus (G_{LT}) and Poisson's ratio (ν_{LT}) is obtained by experimental results, the composite can be fully characterized.

The shear modulus (G_{LT}) is obtained from the torque equation for a rectangular bar:

$$G_{LT} = \frac{M_t}{K_1 \theta (2a)^3 (2b)} \qquad (21)$$

Where:

M_t = (load)(distance) i.e. twisting moment

θ = (angle of twist) ÷ (length of sample)

a = half thickness of sample

b = half width of sample

K_1 = constant obtained from b/a

Poisson's ratio can be calculated from the results obtained when strain, ε, is measured in both the longitudinal and transverse directions for the uniaxial composite. Thus:

$$\nu_{LT} = \frac{\varepsilon_T}{\varepsilon_L} \tag{22}$$

It also holds that:

$$\frac{\nu_{TL}}{\nu_{LT}} = \frac{E_T}{E_L} \tag{23}$$

In deriving stress-strain relationships for a single layer of a laminated composite, it is assumed that the stress normal to the layer is negligible. Thus it results in a plane stress state.

The stress-strain relationship for a lamina in the matrix form is:

$$\begin{bmatrix} \sigma_L \\ \sigma_T \\ \tau_{TL} \end{bmatrix} = \begin{bmatrix} Q_{11} & Q_{12} & 0 \\ Q_{12} & Q_{22} & 0 \\ 0 & 0 & Q_{66} \end{bmatrix} \begin{bmatrix} \varepsilon_L \\ \varepsilon_T \\ \gamma_{LT} \end{bmatrix} \tag{24}$$

Where the components of the stiffness matrix matrix, Q, are:

$$Q_{11} = \frac{E_L}{1-\nu_{LT}\nu_{TL}}$$

$$Q_{22} = \frac{E_T}{1-\nu_{LT}\nu_{TL}} \tag{25}$$

$$Q_{12} = \frac{\nu_{LT}E_L}{1-\nu_{LT}\nu_{TL}}$$

$$Q_{66} = G_{LT}$$

$$Q_{16} = Q_{26} = 0$$

When the stresses are in an arbitrary coordinate system (x, y, z), the following matrix is obtained:

$$\begin{bmatrix} \sigma_X \\ \sigma_Y \\ \tau_{XY} \end{bmatrix} = \begin{bmatrix} \bar{Q}_{11} & \bar{Q}_{12} & 0 \\ \bar{Q}_{12} & \bar{Q}_{22} & 0 \\ 0 & 0 & \bar{Q}_{66} \end{bmatrix} \begin{bmatrix} \varepsilon_X \\ \varepsilon_Y \\ \gamma_{XY} \end{bmatrix} \tag{26}$$

Where the components of the stiffness matrix, $\bar{Q}$, which are now referred to an arbitrary set of axes, are given by:

$$\bar{Q}_{11} = Q_{11}\cos^4\theta + 2(Q_{12} + 2Q_{66})\sin^2\theta\cos^2\theta + Q_{22}\sin^4\theta$$

$$\bar{Q}_{22} = Q_{11}\sin^4\theta + 2(Q_{12} + 2Q_{66})\sin^2\theta\cos^2\theta + Q_{22}\cos^4\theta$$

$$\bar{Q}_{12} = (Q_{11} + Q_{22} - 4Q_{66})\sin^2\theta\cos^2\theta + Q_{12}(\sin^4\theta + \cos^4\theta)$$

$$\bar{Q}_{66} = (Q_{11} + Q_{22} - 2Q_{12} - 2Q_{66})\sin^2\theta\cos^2\theta + Q_{66}(\sin^4\theta + \cos^4\theta)$$

From these equations it is possible to calculate $\bar{Q}_{ij}$ for each layer of the composite.

The laminate constitutive equations are then used to determine the elastic modulus of a multilayer composite. Thus,

$$\begin{bmatrix} F_x \\ F_y \\ F_{xy} \end{bmatrix} = \begin{bmatrix} A_{11} & A_{12} & A_{16} \\ A_{12} & A_{22} & A_{26} \\ A_{16} & A_{26} & A_{66} \end{bmatrix} \begin{bmatrix} \varepsilon_x \\ \varepsilon_x \\ \gamma_{xy} \end{bmatrix} \tag{28}$$

Where:

$$A_{ij} = h_p \sum_{n=1}^{n=N} (\bar{Q}_{ij})_n$$

h_p = thickness of one layer

N = total number of layers

F = force

The modulus of elasticity can be obtained from the equation:

$$E = \frac{1}{h}\left(A_{11} - \frac{A_{12}^2}{A_{22}}\right) \tag{29}$$

where:

h = total thickness of composite

Thermal Expansion

It is possible to calculate the in-plane thermal expansion coefficient in any direction for any laminated panel of proper lamination sequence (i.e. such that no coupling exists through the thickness of the laminate. For each layer above the mid-plane, there is an identical layer in properties and orientation located at the same distance below the mid-plane.) once the elastic properties and the longitudinal (α_L) and transverse (α_T) thermal expansion coefficients are known.

According to reference 4

$$\alpha_1 = \frac{A_{22}R_1 - A_{12}R_2}{A_{11}A_{22} - A_{12}^2}$$

$$\alpha_2 = \frac{A_{11}R_2 - A_{12}R_1}{A_{11}A_{22} - A_{12}^2}$$

Where:

$$R_1 = J_1 h + J_2 H_1$$

$$R_2 = J_1 h - J_2 H_1$$

$$A_{11} = U_1h + U_2H_1 + U_3H_2$$

$$A_{22} = U_1h - U_2H_1 + U_3H_2$$

$$A_{12} = U_4h - U_3H_2$$

$$J_1 = (U_1 + U_4)W_1 + 2U_2W_2$$

$$J_2 = (U_2W_1 + 2W_2)(U_1 + 2U_3 - U_4)$$

$$W_1 = 1/2(\alpha_L + \alpha_T)$$

$$W_2 = 1/4(\alpha_L - \alpha_T)$$

$$H_1 = \sum_{n=1}^{N} h_n \cos 2\theta_n$$

$$H_2 = \sum_{n=1}^{N} h_n \cos 4\theta_n$$

where h is the laminate thickness, N is the number of layers, θ_n is the angle between the 1 axis (direction in which expansion coefficient is calculated) and the fibers in the nth layer and h_n is the thickness of the nth layer.

$$U_1 = 1/8(3Q_{11} + 3Q_{22} + 2Q_{12} + 4Q_{66})$$

$$U_2 = 1/2(Q_{11} - Q_{22})$$

$$U_3 = 1/8(Q_{11} + Q_{22} - 2Q_{12} - 4Q_{66})$$

$$U_4 = 1/8(Q_{11} + Q_{22} + 6Q_{12} - 4Q_{66})$$

and

$$Q_{11} = E_L/(1 - \nu_{LT}\nu_{TL})$$

$$Q_{22} = E_T/(1 - \nu_{LT}\nu_{TL})$$

$$Q_{12} = \nu_{LT}E_T/(1 - \nu_{LT}\nu_{TL})$$

$$Q_{66} = G_{LT}$$

$$\nu_{TL} = \nu_{LT}E_T/E_L$$

In the case of an isotropic (in plane) laminate this reduces to:

$$\alpha_1 = \alpha_2 = \frac{J_1}{U_1 + U_4}$$

Thermal Stresses

Assuming a temperature change of one degree centigrade, the thermal expansion of "free" strain of the individual layer will be $\varepsilon_L = \alpha_L$ and $\varepsilon_T = \alpha_T$ in the longitudinal and transverse directions of that layer. The thermal expansion strain of the layer or ply in the 1 and 2 directions is given by:

$$\varepsilon_{1p} = \varepsilon_L \cos^2\theta + \varepsilon_T \sin^2\theta$$
$$\varepsilon_{2p} = \varepsilon_L \sin^2\theta + \varepsilon_T \cos^2\theta$$
$$\varepsilon_{12p} = (\varepsilon_L - \varepsilon_T)\sin^2\theta$$

since the layers expand like the rest of the composite by an amount $\varepsilon_{1c} = \alpha_1$ and $\varepsilon_{2c} = \alpha_2$ in the 1 and 2 directions. The difference between the "free" and constrained expansion is a strain that is associated with a stress. The stress associated with these strains is:

$$\sigma_1 = \overline{Q}_{11}\varepsilon_1 + \overline{Q}_{12}\varepsilon_2 + \overline{Q}_{16}\varepsilon_{12}$$
$$\sigma_2 = \overline{Q}_{12}\varepsilon_1 + \overline{Q}_{22}\varepsilon_2 + \overline{Q}_{66}\varepsilon_{12}$$
$$\sigma_{12} = \overline{Q}_{16}\varepsilon_1 + \overline{Q}_{26}\varepsilon_2 + \overline{Q}_{66}\varepsilon_{12}$$

where:

$$\overline{Q}_{11} = U_1 + U_2\cos 2\theta + U_3\cos 4\theta$$
$$\overline{Q}_{12} = U_4 - U_3\cos 4\theta$$
$$\overline{Q}_{66} = U_5 - U_3\cos 4\theta$$
$$\overline{Q}_{16} = (-1/2)U_2\sin 2\theta - U_3\sin 4\theta$$
$$\overline{Q}_{26} = (-1/2)U_2\sin 2\theta + U_3\sin 4\theta$$

What is actually needed is to obtain the stresses in the individual layers referred to the longitudinal and transverse axes of the layer rather than the 1, 2 axes.

Thus the transformation equations:

$$\sigma_L = \sigma_1 \cos^2\theta + \sigma_2 \sin^2\theta + \sigma_{12} \sin 2\theta$$

$$\sigma_T = \sigma_1 \cos^2\theta + \sigma_2 \sin^2\theta - \sigma_{12} \sin 2\theta$$

$$\sigma_{LT} = 1/2(\sigma_2 - \sigma_1)\sin 2\theta + \sigma_{12} \cos 2\theta$$

EXPERIMENTAL PROCEDURE

Fabrication

Samples were made from epoxy pre-impregnated PAN-based graphite sheets obtained from Monsanto. These sheets consisted of Monsanto resin type 4617/mPDA with a 55 w/o fiber. The sheets, originally 0.61m x 1.22m, were cut into 15.2cm squares. The squares were cut so that the fiber axis was at 0^o or 90^o with the edge of the square for the unidirectional and the $[[\pm 45_3]_2]_T$ samples and at 0^o, 30^o, and 60^o for the $[0/30/60/90/-60/-30]_S$ sample.

Twelve-layer samples were made for each of the following orientation sequences:

Layer Number		1	2	3	4	5	6	7	8	9	10	11	12
Angle in degrees	I	0	0	0	0	0	0	0	0	0	0	0	0
	II	+45	-45	+45	-45	+45	-45	+45	-45	+45	-45	+45	-45
	III	0	30	60	90	-60	-30	-30	-60	90	60	30	0

The first layup will be referred to as unidirectional, the second as $[[\pm 45_3]_2]_T$ and the third as $[0/30/60/90/-60/-30]_S$. The layers were then placed in a mold fitted with a die and punch. The mold was then placed between the platens of the hot press where a pressure of 345 kN/m^2 and a temperature of 353 K were applied (Figure 2). At the end of two hours the pressure was increased to 690 kN/m^2 and the temperature was increased to 423 K. The samples were then cured an additional two hours. After the samples were properly cured the hot press was turned off and the samples were cooled to room temperature by water flowing through the platens.

Once the samples were removed from the mold, they were checked for any visible flaws and the thickness was measured. The final sample measured 15.2cm x 15.2cm x 0.20cm.

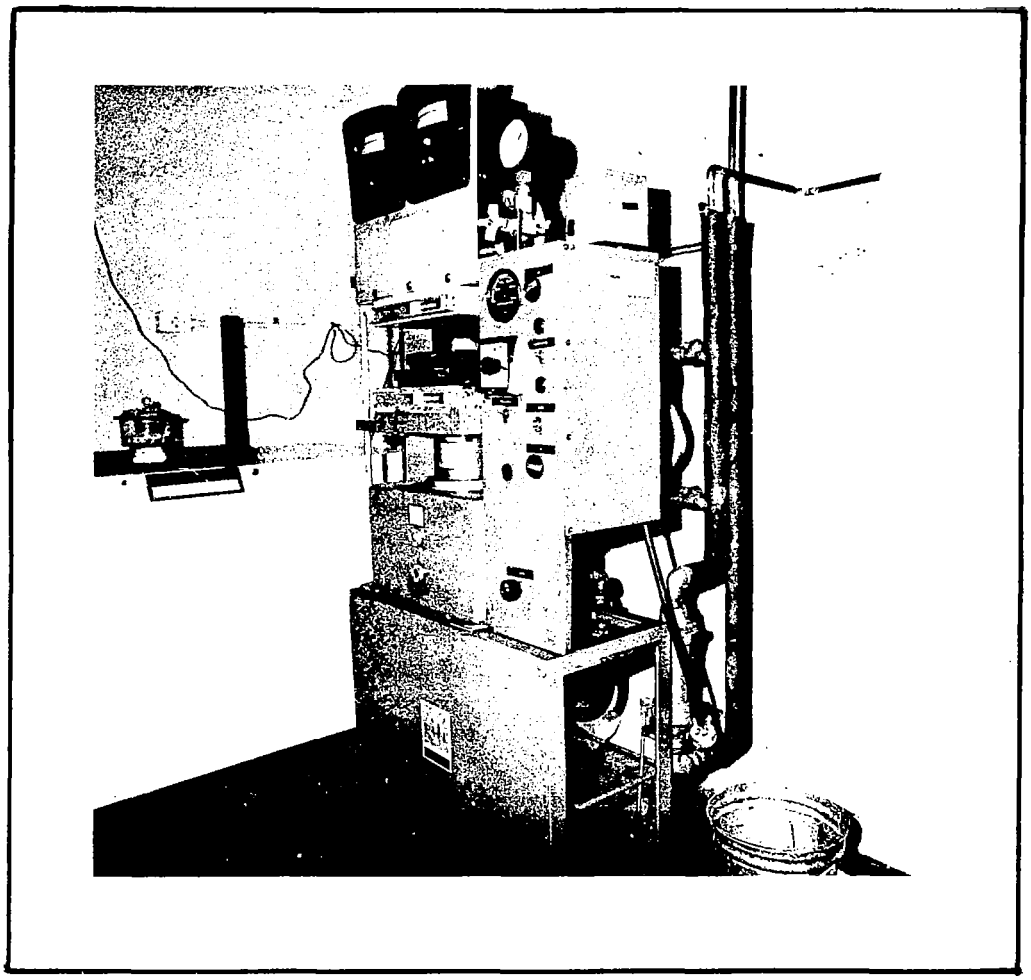

Figure 2. Hot Press

Microscopic Examination

To prevent time being wasted by testing poor samples, each sample was examined microscopically. Two cross sections of each sample, cut at right angles to one another, were examined under the microscope. The purpose of the examination was to ascertain the fiber orientation in each layer, to check thickness, and parallelism of the individual layers as well as the uniformity of fiber distribution and general integrity of the composite.

Once the samples were cycled, they were again examined under the microscope to determine what changes if any occurred during the thermal cycling.

Modulus of Elasticity

The proposed work in mechanical properties consisted of measuring the elastic modulus in the 0° direction of the three different composite configurations. Later it was decided that a complete characterization of the material was needed. This characterization required measuring the longitudinal modulus (E_L), the transverse modulus (E_T), the shear modulus (G_{LT}), and Poisson's ratio (ν_{LT}) of the unidirectional sample. From these values E_L, E_T, G_{LT}, ν_{LT} the elastic modulus of any composite with any construction can be calculated and compared with experimantal results.

Specimens, approximately 1.27cm x 7.6cm x 0.20cm, were cut from the samples. To insure that an even load was applied to the specimens and that the specimens were not damaged by the jaws of the testing machine, aluminum strips were glued to each side of the sample with epoxy at both ends.

All samples were loaded in tension with the load and strain being recorded. The accumulated strains were recorded by the use of SR-4 strain gages and a strain gage recorder, both produced by BLH Electronics. The strain gages were attached to the unidirectional specimens so that each gage was at 0^{o} with the fiber axis to measure ε_{L}, and at 90^{o} to measure ε_{T}. Two measurements were taken on the $[[\pm 45_3]_2]_T$ sample, one with the strain gage oriented in either the $+45^{o}$, or -45^{o} direction and the other along the 0^{o} axis. The applied load was read directly from the Tinus-Olsen Testing Machine.

Due to the small loads required to break the unidirectional 90^{o} specimens, the modulus of elasticity was obtained from a four point flexure test. The strain was obtained from strain gages and the applied load from loads placed on the testing apparatus.

Poisson's ratio was calculated using a dual strain gage that was attached to the unidirectional specimens. The shear modulus was measured using the method of torque applied to a rectangular bar.

Determination of Thermal Expansion

The coefficient of thermal expansion was determined for each panel with different construction. One specimen was cut from the $[[\pm 45_3]_2]_T$ and the $[0/30/60/90/-60/-30]_S$ panel since the thermal expansion should be the same in all directions in these two panels (6). The specimens from the unidirectional samples were taken such that the following angles were made with the unidirectional axis:

Angle in Degrees 0, 15, 30, 45, 60, 75, and 90

The ends of the specimens were ground flat, parallel and perpendicular to the specimen axis.

Each specimen was slowly heated in a dilatometer, Figure 3, from room temperature to 453K at the approximate rate of 1° K/minute. The specimens were then cooled to room temperature by cutting off the heating current. While the first heating and cooling curves showed hysteresis, further heating followed very closely the cooling curve and the behavior became essentially reversible. The thermal expansion coefficient was determined from the cooling cycle and was measured between 323K and 423K.

Once the samples were cycled, each was again measured for thermal expansion and compared to the uncycled values.

Ultimate Tensile Strength

Samples used to calculate elastic modulus were loaded until fracture to obtain the ultimate tensile strength.

Scanning Electron Microscope

The fracture surfaces of the ultimate tensile test samples were observed using the electron microscope. The samples were mounted in an aluminum split-ring holder. Even though the samples had an epoxy surface, there was enough exposed graphite touching the holder to allow electrical conduction, therefore eliminating the need to carbon coat the sample.

The entire surface of the fracture was observed and photomicrographs were taken of areas of special interest.

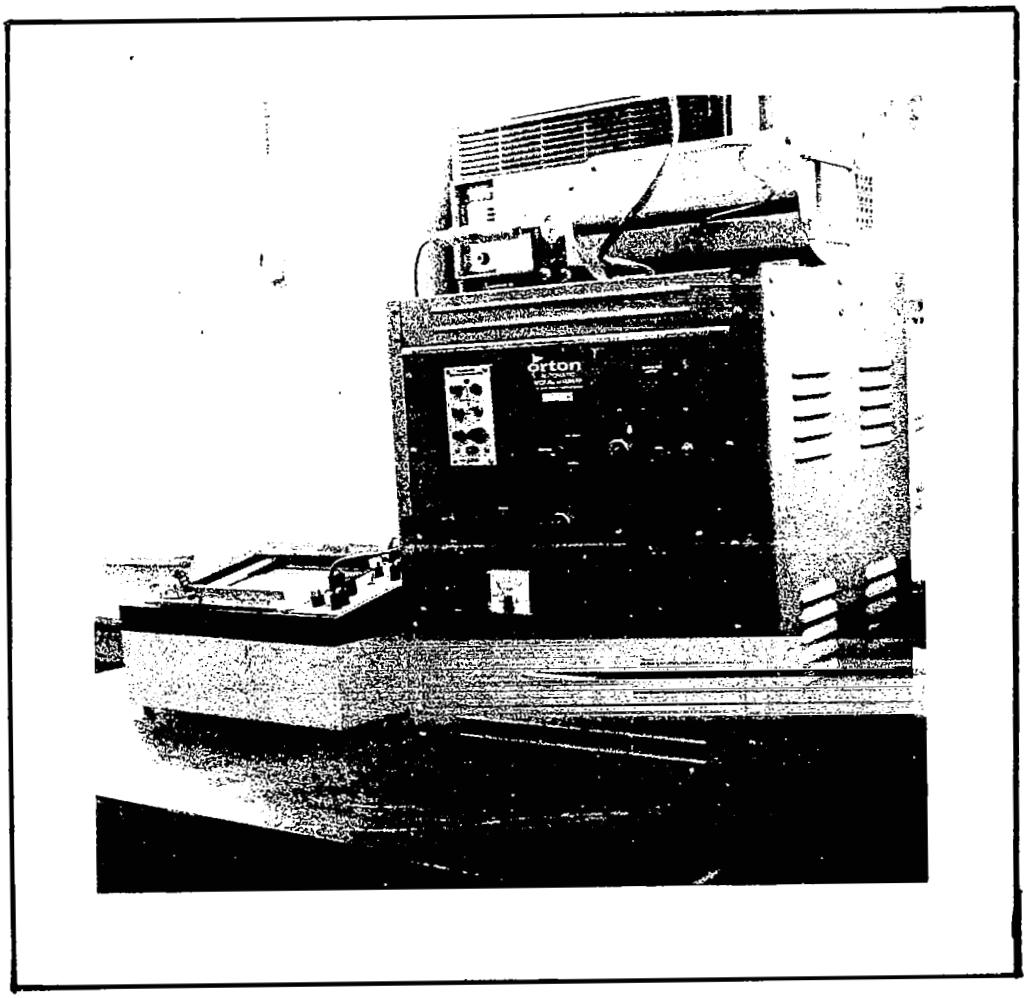

Figure 3. Dilatometer

Thermal Cycling

Since it was proposed that test samples be cycled in the range 223K to 423K for as many as 10,000 cycles and without thermal shock, an automatic cycling device had to be developed.

The first step in developing the cycling device was to determine how to obtain the desired temperature. After some experimentation it was determined that resistance heating and liquid nitrogen flowing through a copper coil would give the desired temperature.

Since moisture condensation would be a problem if the samples were cycled in air, it was decided that the samples would either be cycled in a vacuum or in a dry atmosphere.

The requirement that the sample be cycled in a controlled atmosphere or vacuum along with the selected type of heating and cooling methods dictated that the cycling chamber be a closed system with an external method of moving the sample from the hot to cold environment.

A 5-cm diameter by 1.22-m long piece of boro-silicate glass tubing was selected as the cycling chamber. The hot end was made by wrapping chromel wire around the tube and topping it with Saverisn Cement and asbestos tape. By connecting the wire to a variable transformer, the temperature at the hot end could be varied from room temperature to 523K (Figure 4).

The cold end of the chamber was made by coiling 9m of 0.64-cm OD copper tubing so that it just fitted around the glass tube. A tank

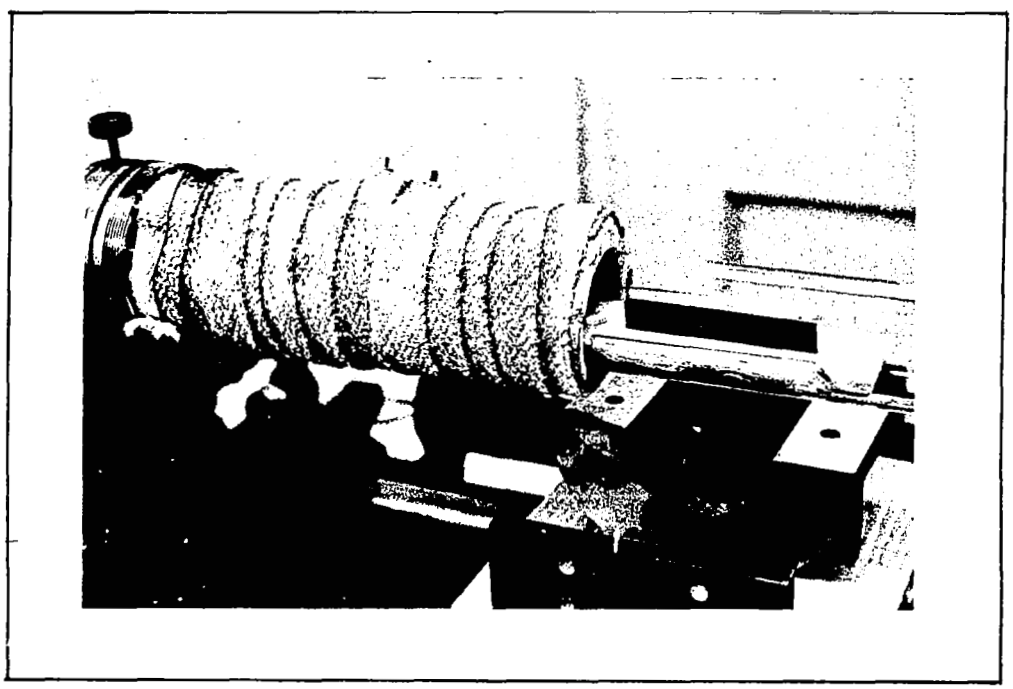

Figure 4. Hot End of Cycling Device

of liquid nitrogen was connected to the tubing and the valve was adjusted so that only nitrogen gas would flow (Figure 5).

The distance between the hot end and cold end was approximately 0.61 m. This distance allowed the middle of the chamber to remain at room temperature and reduced the chance of thermal shock in the sample. The ends of the tube were fitted with two-hole rubber stoppers. One hole on each end was used for a thermocouple and the other for an outlet pipe that was connected to a vacuum pump. The tube was then tested and it was found that the desired temperatures (223K to 423K) could be maintained.

Since the chamber was a closed system, a method of cycling the samples without disturbing the vacuum had to be developed. It was determined that if the sample holder were made of steel, that a magnet outside the tube could move the sample holder from one end to the other. It was found that a solid steel holder was too heavy to be moved easily by the magnet and it was easy to accidentally break the glass tube with such a holder. The next sample holder was made of Teflon with grooves cut into it to carry eight 1.27cm x 7.6cm x 0.20cm samples. A piece of steel was inserted into the bottom of the holder. Too much drag was developed by the Teflon being dragged against the glass tube causing the sample holder to move in jerks or even become stuck. The final design consisted of placing the Teflon holder in a piece of 4.76-cm diameter glass tubing that had been longitudinally cut in half. This holder allowed sliding contract between two glass surfaces (Figure 6). To reduce friction, 200-micron glass beads were used as a lubricant.

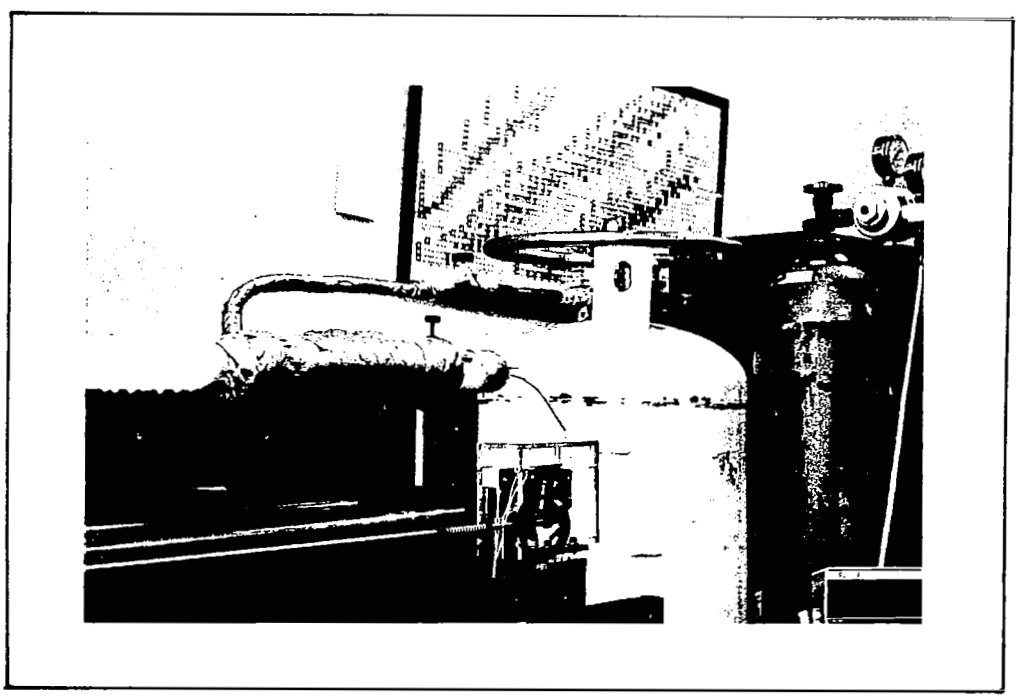

Figure 5. Cold End of Cycling Device

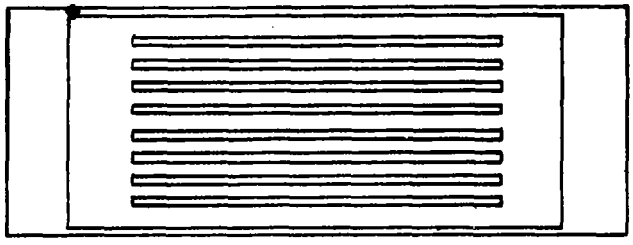

Top View

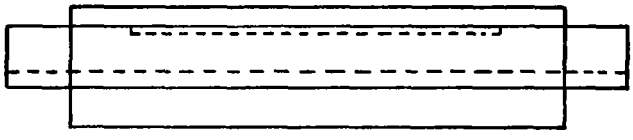

Side View

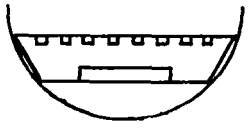

End View

Figure 6. Sample Holder

The final step in constructing the thermal cycling apparatus was to develop a method of moving the magnet under the glass tube back and forth so that it would pull the sample holder from one end to the other. It was decided to modify a zone refining machine to produce the desired apparatus. The zone refining machine already had a reversing motor, a carriage system, and a rod that could be used to trip microswitches. The first step in converting the zone refiner was to build a controller for the reversing motor that would allow the samples to remain at each end until they had reached the required temperature. This was accomplished by the use of a capacitor buildup system. As the carriage traveled to one end, it would trip a microswitch. This allowed a capacitor to start charging and when the charge was complete, the carriage was released. The carriage traveled to the other end where it hit another microswitch and the entire process started again. The controller had a variable resistor that allowed the time period for capacitor buildup to be varied. This allowed the sample to remain at either end for a predetermined period of time.

Once the cycling apparatus was completed, a thermocouple placed inside a sample was cycled to determine how much time would be required at each end to heat and cool the sample. The first sample required a total cycle time of 25 minutes. The heating took six minutes and the cooling 19 minutes. Since this was an unrealistically long time, the tube was redesigned so that the wasted nitrogen gas could be fed into the tube (Figure 7). By having the gas blow over the samples, it not only cooled the sample quicker, but provided a dry atmosphere in which

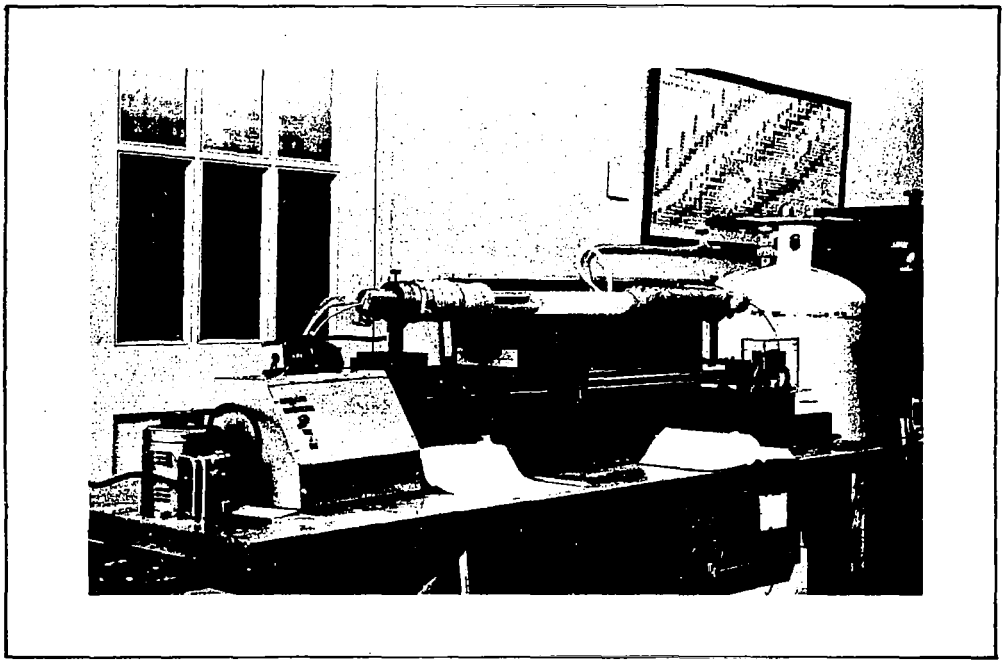

Figure 7. Thermal Cycling Device

the sample could be cycled. The design allowed the gas to escape from the cold end without flowing to the hot end. The nitrogen also acted as a heat conductor thus allowing the samples to be heated quicker. The thermocouple was then cycled again and it was found that the total cycling time could be cut to 5 minutes.

Two other modifications were later made. One was to place a piece of bronze in the cold end to be used as a heat sink and the other was to purge the chamber with helium before the nitrogen was introduced. The first step reduced the amount of liquid nitrogen used and the second step kept moisture from condensing inside the tube.

RESULTS AND DISCUSSION

Microscopic Examination

Figures 8, 9, and 10 show the photomicrographs of the uncycled fiber composites.

Figure 8 is the unidirectional sample. The top micrograph shows the fibers in cross-section. Four fiber layers are distinguishable even though there is good bonding between and good fiber distribution in the layers. The second two micrographs were taken parallel to the fibers.

Figure 9 is a micrograph of the $[[\pm 45_3]_2]_T$ sample. There is good bonding between layers and little or no transverse cracking.

Figure 10 is of the $[0/30/60/90/-60/-30]_S$ sample. The top micrograph shows seven layers starting with the 0^o direction and ending with two 30^o directions. The six layers on top represent one-half of the thickness (the mid plane is marked on the photomicrograph by a dark line. The construction of the bottom half is identical to that of the upper half). The other two micrographs taken at higher magnification show the fiber cross sections in different layers. Good bonding with practically no cracking was observed for this configuration.

Figures 11 through 14 show the composite material after cycling. The top micrograph in each figure was taken after ten cycles with the following micrographs taken after 100, 1000, and 5000 cycles in this order.

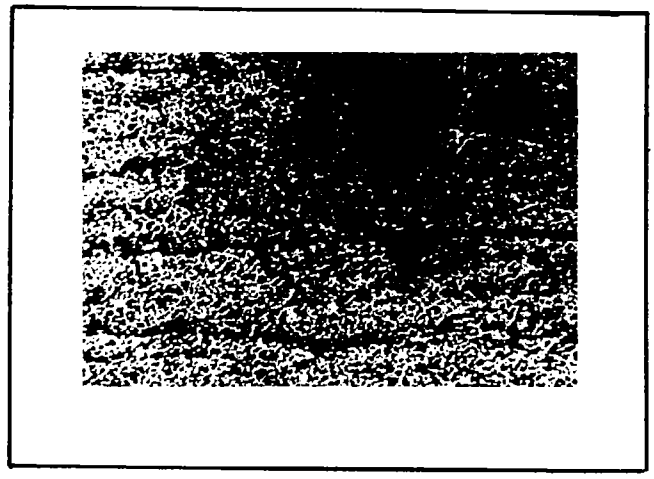

100X

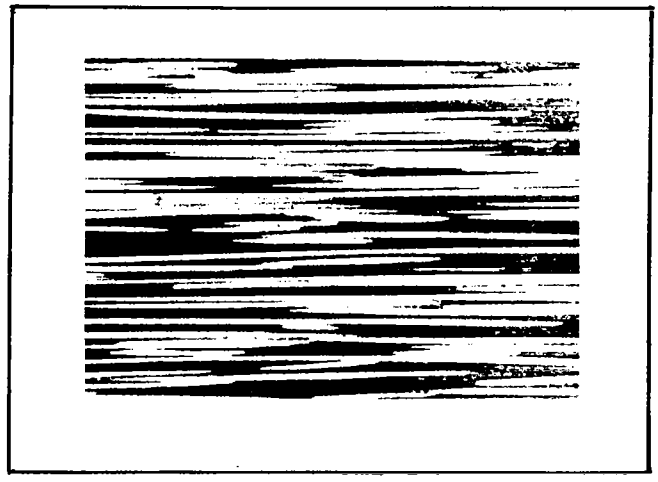

150X

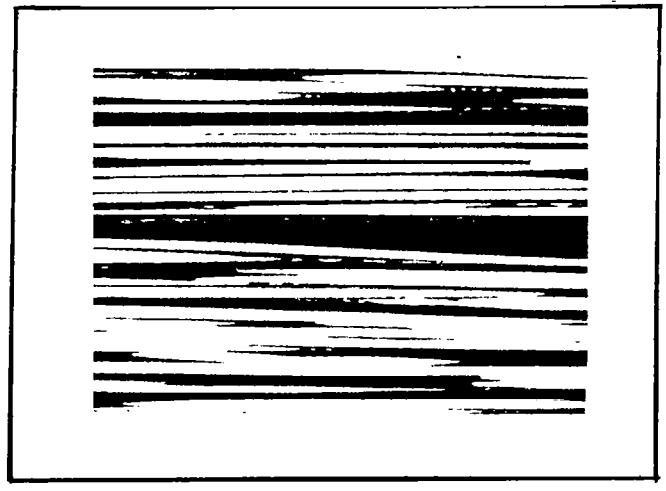

300X

Figure 8. Uncycled Unidirectional Sample

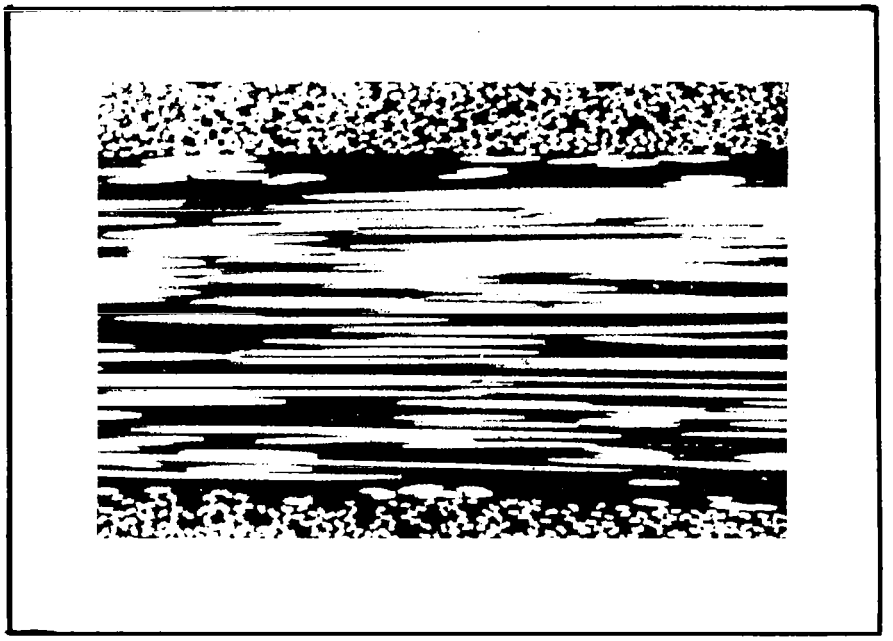

Figure 9. Uncycled $[[\pm 45_3]_2]_T$ Sample, 300X

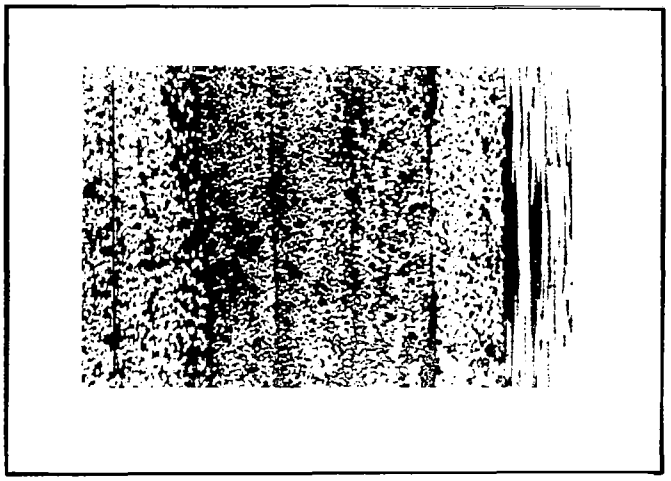

100X

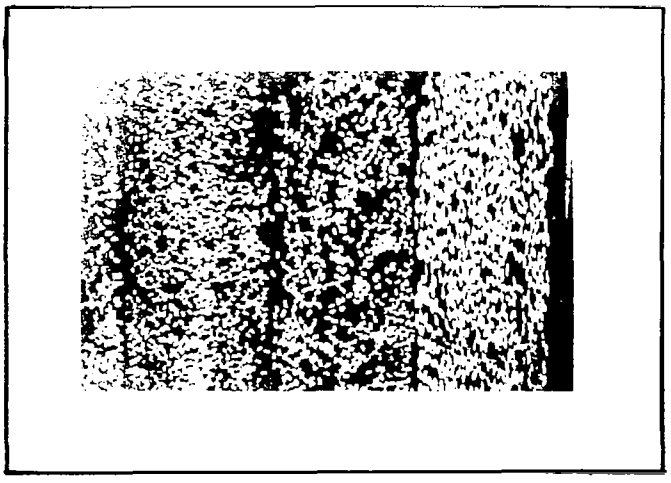

150X

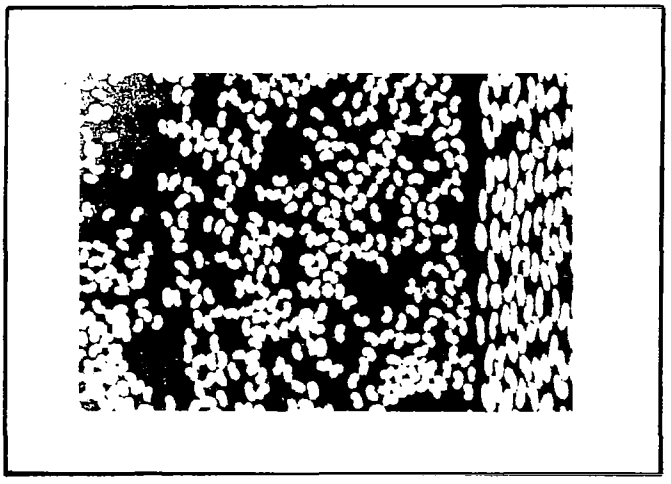

350X

Figure 10. Uncycled $[0/30/60/90/-60/-30]_S$ Sample

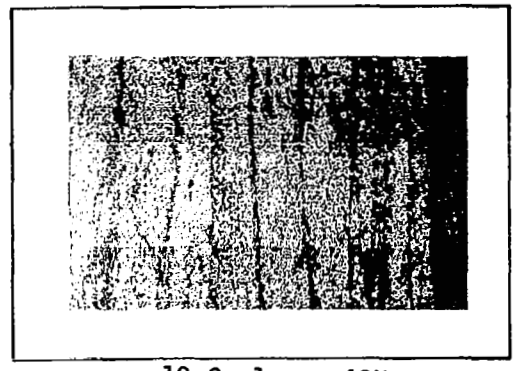

10 Cycles 40X

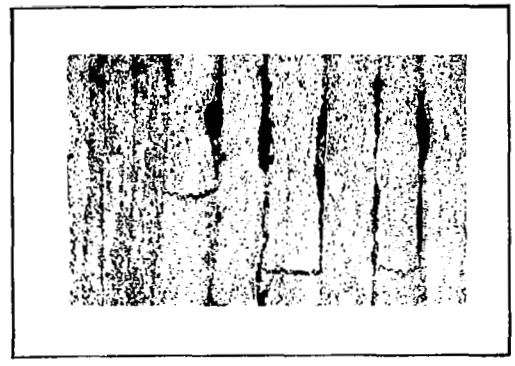

100 Cycles 40X

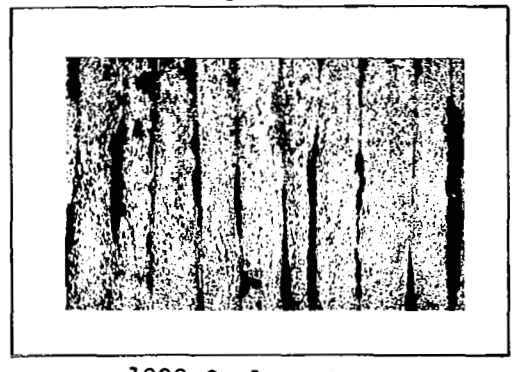

1000 Cycles 40X

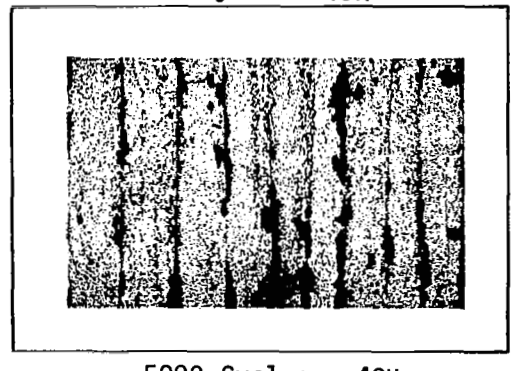

5000 Cycles 40X

Figure 11. Cycled $[[\pm 45_3]_2]_T$ Sample, Photomicrographs Taken Along 0^o Axis

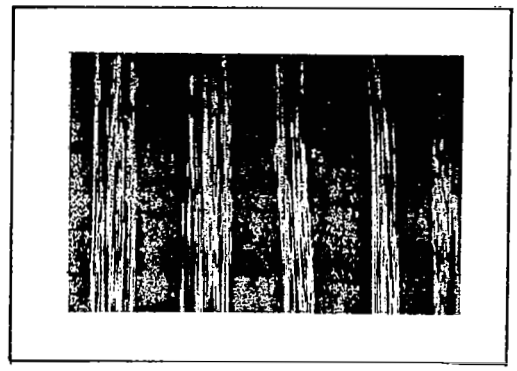

10 Cycles 40X

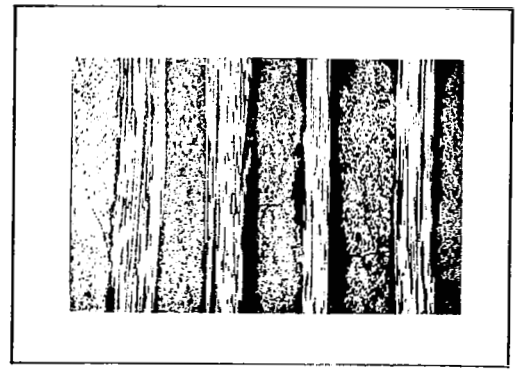

100 Cycles 40X

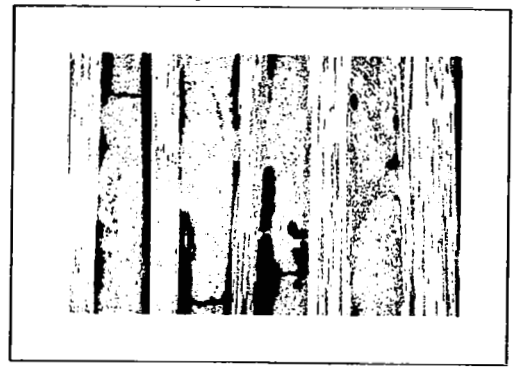

1000 Cycles 40X

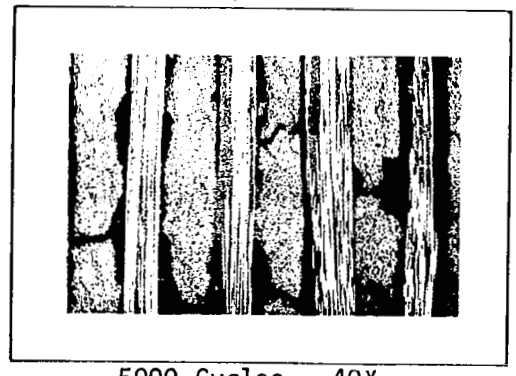

5000 Cycles 40X

Figure 12. Cycled $[[\pm 45_3]_2]_T$ Sample, Photomicrographs Taken Along Fiber Axis

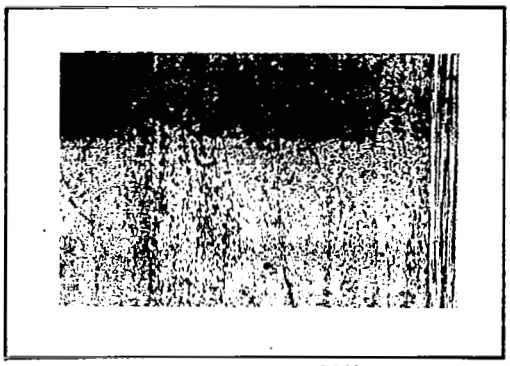

10 Cycles 40X

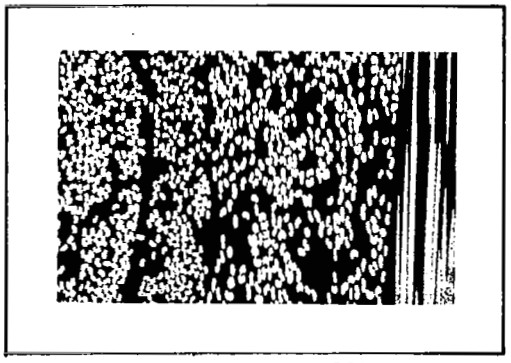

100 Cycles 40X

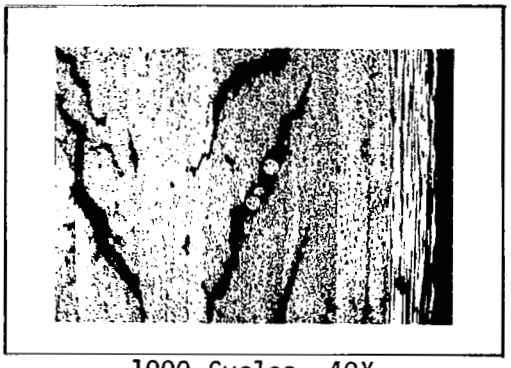

1000 Cycles 40X

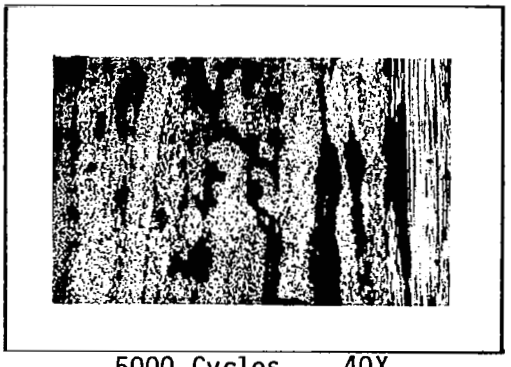

5000 Cycles 40X

Figure 13. Cycled $[0/30/60/90/-60/-30]_s$ Sample

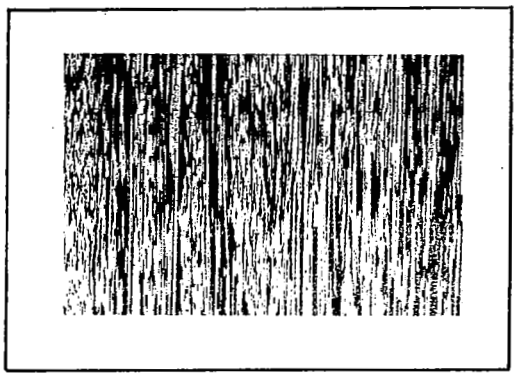

10 Cycles 40X

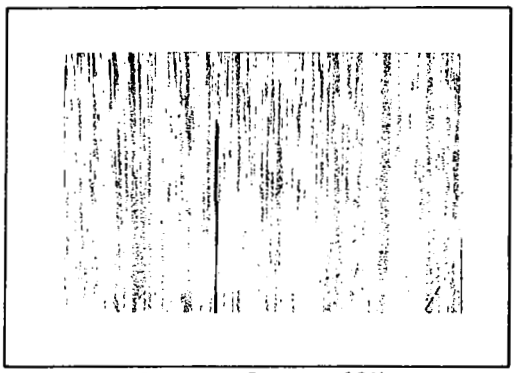

100 Cycles 40X

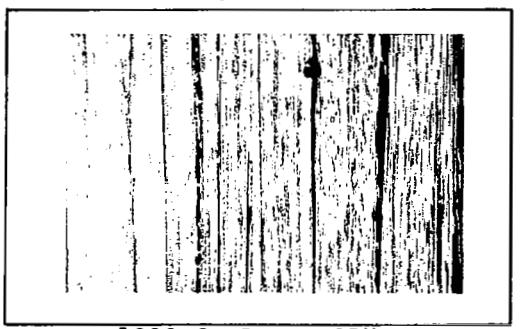

1000 Cycles 40X

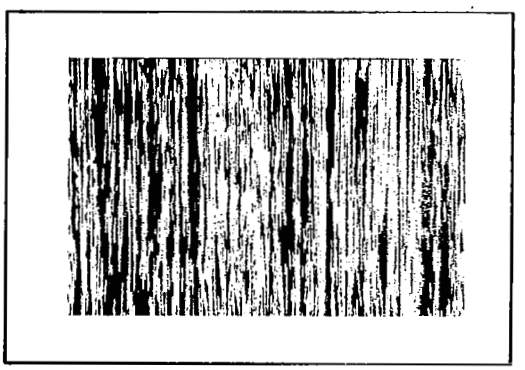

5000 Cycles 40X

Figure 14. Cycled Unidirectional Sample

Figures 11 and 12 are both of the $[[\pm 45_3]_2]_T$ sample. Figure 11 was taken along the 0^o axis while Figure 12 was taken along the fiber axis. The micrographs indicate that transverse cracking starts with as few as ten cycles while delamination does not appear until 100 cycles. As the number of cycles increased, the severity and number of transverse cracks as well as the severity of delamination increased.

Figure 13 is the $[0/30/60/90/-60/-30]_s$ sample. The cracking after 10 or 100 cycles does not appear to be nearly as severe as it was in the $[[\pm 45_3]_2]_T$ sample. The type of cracking in the sample is very different from that found in the $[[\pm 45_3]_2]_T$ sample. Instead of the crack being stopped at the boundary between two plys, the crack is able to cross the boundary and continue into the next layer. This could be due to the slight angle between layers as compared to the $[[\pm 45_3]_2]_T$ sample. The crack extends to the boundary, proceeds along a partial delamination between layers, and then continues into the next layer. This pattern can be clearly seen in the 1000 cycle photomicrograph, but is not very distinguishable in the 5000 cycle micrograph due to the severe cracking.

Figure 14 is the photomicrograph of the unidirectional sample. The first 100 cycles had little effect on the sample, but further cycling caused deterioration through delamination.

As can be seen from the photomicrographs, the unidirectional composites are normally free from cracks as prepared. The fiber-matrix interaction stresses which result from the disparity of thermal expansion and from the curing shrinkage of the matrix are apparently not high enough

to induce cracking, especially when at the curing temperature the matrix can easily flow to relieve the curing shrinkage stresses. Laminate composites on the other hand usually contain transverse cracks. These cracks are due to the thermal expansion mismatch stresses between layers. In a sense these are macrostresses encompassing the entire layer, while the fiber-matrix stresses are microstresses. Some workers believe that curing shrinkage may also contribute to such transverse cracking (7). However, in the samples prepared for this work there were no cracks in the unidirectional composites and very few transverse cracks in the laminated composites. Some were practically free of any cracking. This is attributed to the care with which the samples were prepared and particularly to the very slow cooling following the cure. This tends to indicate that it is the thermal mismatch rather than the curing shrinkage that is primarily responsible for the often observed transverse cracks in the laminated composites. Any cracking that occurred later upon thermal cycling can clearly be attributed to thermal stresses.

The structural damage that occurred in the composites as a result of thermal cycling may be summarized as follows:

(1) In the unidirectional sample, which contained no cracks or defects at the start of cycling, cracks gradually developed parallel to the fibers. The number of cracks was small, but increased with the number of cycles. It is believed that they are at the surfaces separating the preimpregnated sheets from which the composite was constructed. The cracking (which in this case amounts to delamination)

may be due to thermal stress resulting from two sources: (a) a very slight misorientation of the fibers in adjacent sheets (or even within the sheets) which from a practical standpoint cannot be completely avoided and (b) a slight difference in volume fraction of fibers at the junction of the pre-impregnated sheets. This minor defect is also practically impossible to avoid especially if the misorientation described in (a) is present.

(2) In the $[[\pm 45_3]_2]_T$ composite, i.e., in the composite with the maximum change of orientation between layers, the damage resulting from thermal cycling can be described as follows:

a. Development of transverse cracks:
The crack surfaces are parallel to the fibers in the individual layer and hence their direction in one layer makes a right angle with their direction in the next. The cracks in one layer seem to be unrelated to those in the next.

b. Delamination of the composite:
This consisted of a separation between layers and again seems to be unrelated to the transverse cracks in the same that they do not extend between individual cracks.

(3) In the $[0/30/60/90/-60/-30]_S$ sample i.e., in the composite with the least drastic change in orientation, the damage consisted of cracks which propagated across layer interfaces with very little, if any delamination. In cases where delamination was detected, it was clearly associated with the cracks and actually constituted a part of the crack as it propagated from one layer to another.

Modulus of Elasticity

The strain and load data taken during the testing was plotted and a best fit line was drawn. From this the modulus, E, was calculated using:

$$E = \frac{\frac{\text{load}}{\text{area}}}{\text{strain}}$$

This was done on all specimens except the transverse unidirectional specimen where four point bending was used. The modulus in this case is given by the formula:

$$E = \frac{3P}{2bh^2\varepsilon}$$

Where:

E = elastic modulus

P = applied load

b = width of specimen

h = thickness of specimen

ε = strain

and the distance between knife edges in the four point bending test was 5.08cm.

Using formulas 1 and 7 contained in the theoretical section, the modulus for the unidirectional was calculated. E_L was 191×10^9 N/m^2 and E_T was 7.6×10^9 N/m^2. These values compare very favorably with the E_L of 182×10^9 N/m^2 and E_T of 6.8×10^9 N/m^2 obtained experimentally.

The experimental values obtained for E_L, E_T, G_{LT}, and ν_{LT} were used to calculate the theoretical values for the $[[\pm 45_3]_2]_T$, and the $[0/30/60/90/-60/-30]_S$ composites. The values were:

For the $[[\pm 45_3]_2]_T$ samples:

Along the fiber axis (either $+45^o$, -45^o) $E = 9.48 \times 10^{10}$ N/m^2

Along the 0^o axis $E = 1.37 \times 10^{10}$ N/m^2

For the $[0/30/60/90/-60/-30]_s$ sample: $E = 6.23 \times 10^{10}$ N/m^2

The $[[\pm 45_3]_2]_T$ sample had an experimentally determined modulus of 7.81×10^{10} N/m^2 when tested in either the +45° or -45° direction and 1.47×10^{10} N/m^2 when measured at 0^o. These values compared fairly well with the 9.48×10^{10} N/m^2 and the 1.37×10^{10} N/m^2 moduli calculated.

The $[0/30/60/90/-60/-30]_s$ specimen should have the same modulus in all directions. The modulus measured was 5.72×10^{10} N/m^2 as compared to the calculated value of 6.23×10^{10} N/m^2.

The calculate values were higher than the experimental values in most cases. This could be due in part to the specimen not being tested exactly along the designated axis. It is easy to see the dramatic reduction in modulus in the $[[\pm 45_3]_2]_T$ specimen when the tensile axis is moved away from the fiber axis.

Table I is a tabulation of all the experimental elastic moduli data. It can be seen that the most dramatic change in tensile modulus for all samples occurs during the first ten cycles. After the first ten cycles, further cycling seems to cause little or no more damage.

Sample Type		Unidirectional	$[[0/30/60/90/-60/-30]_S$	$[[\pm 45_3]_2]_T$	
Test Direction		0^o	0^o	0^o	45^o
Number of Cycles	0	18.2×10^{10}	5.7×10^{10}	1.4×10^{10}	7.8×10^{10}
	10	14.3×10^{10}	5.0×10^{10}	1.3×10^{10}	7.0×10^{10}
	100	15.1×10^{10}	5.0×10^{10}	1.4×10^{10}	7.2×10^{10}
	1000	13.2×10^{10}	4.2×10^{10}	1.2×10^{10}	7.2×10^{10}
	5000	14.5×10^{10}	4.6×10^{10}		7.1×10^{10}

Table I. Modulus of Elasticity of Graphite-Epoxy Composite Material. Values given in N/m^2.

Thermal Expansion

The thermal expansion coefficient α of the quasi-isotropic samples (i.e. $[[\pm 45_3]_2]_T$ and the $[0/30/60/90/-60/-30]_S$ were very close. The value of this coefficient α for the $[[\pm 45_3]_2]_T$ sample was $1.6 \times 10^{-6}/^{o}K$ as compared to $2.2 \times 10^{-6}/^{o}K$ for the $[0/30/60/90/-60/-30]_S$ sample. Considering the values are subject to an experimental error as much as $\pm 0.5 \times 10^{-6}/^{o}K$, the values could be considered to be the same. It can be seen that these values of the coefficients are very small when one considers that a unidirectioned composite of the same material and proportions yields a transverse coefficient of $69.7 \times 10^{-6}/^{o}K$.

The unidirectional sample showed a clear trend for the expansion coefficient to increase as the angle between the fiber axis and specimen axis increased from 0^{o} to 90^{o}. This is shown in Figure 15. The simple formula for a homogeneous orthotropic material is $\alpha_c = \alpha_{0^o}\cos^2\theta + \alpha_{90^o}\sin\theta$ and the experimental results show a good correlation with this formula.

It was found that once the composite material was cycled, that the amount of thermal expansion was lower in all cases. The α for the $[[\pm 45_3]_2]_T$ sample was $0.5 \times 10^{-6}/^{o}K$ as compared to $1.6 \times 10^{-6}/^{o}K$ measured before cycling. The α for the $[0/30/60/90/-60/-30]_S$ sample had an average value of $0.65 \times 10^{-6}/^{o}K$ as compared to the uncycled value of $2.2 \times 10^{-6}/^{o}K$. The unidirectional sample was tested only in the transverse direction. It was found that the α for this sample remained about the same as the uncycled samples until approximately 1000 cycles. The value of α then dropped slightly to a value of $67.4 \times 10^{-6}/^{o}K$. The above results are summarized in Table II.

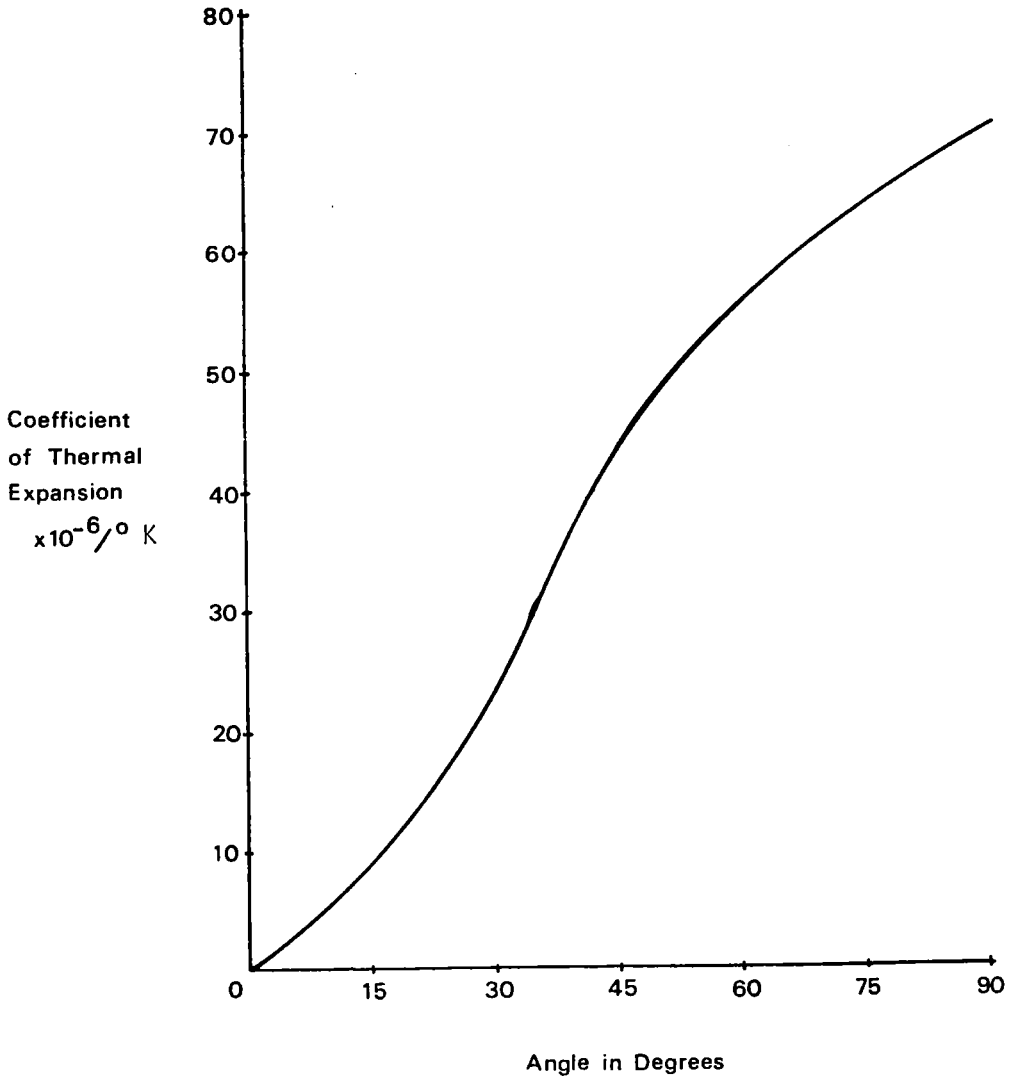

Figure 15. Thermal Expansion vs Angle from Fiber Direction in Unidirectional Sample

Sample Type	Unidirectional		$[0/30/60/90/-60/-30]_S$	$[[\pm 45_3]_2]_T$
Test Direction	0^o	90^o	0°	0°
Uncycled	$-0.3 \times 10^{-6}/^oK$	$69.7 \times 10^{-6}/^oK$	$2.20 \times 10^{-6}/^oK$	$1.60 \times 10^{-6}/^oK$
After 1000 cycles		$67.4 \times 10^{-6}/^oK$	$0.65 \times 10^{-6}/^oK$	$0.50 \times 0^{-6}/^oK$

Table II. Thermal Expansion Coefficients of Graphite-Epoxy Composite Material

Sample Type		Unidirectional	$[[\pm 45_3]_2]_T$		$[0/30/60/90/-60/-30]_S$
Test direction:		0^o	0^o	45^o	0^o
Number of Cycles	0	234.4×10^6	106.7×10^6	188.9×10^6	167.5×10^6
	10	120.3×10^6	63.5×10^6	61.0×10^6	86.2×10^6
	100	150.8×10^6	59.5×10^6	80.7×10^6	79.3×10^6
	1000	175.6×10^6	72.3×10^6	115.1×10^6	127.6×10^6
	5000	162.2×10^6			49.3×10^6

Table III. Ultimate Tensile Strength of Graphite-Epoxy Composite Material. Values are given in N/m^2.

Thermal Stresses

In the unidirectional sample, thermal stresses between layers are not present. Although the composite is constructed of many preimpregnated sheets, it may be considered a single layer.

A state of stress was noted in the $[[\pm 45_3]_2]_T$, and $[0/30/60/90/-60/-30]_S$ samples. Calculations showed the stress to be $+0.45 \times 10^6$ and -0.45×10^6 N/m^2/K in the longitudinal and transverse directions of the layers with all layers being identical. Of course the strain is much lower in the longitudinal direction, but the modulus is much higher than in the transverse direction. As the temperature rises, a tensile stress is developed in the longitudinal direction while a compressive stress is developed in the transverse direction. As the temperature drops, just the opposite is true.

A drop in temperature from the high end of the temperature range (423K) to the low end (223K) of the range used in this study would cause a tensile stress buildup of 90×10^6 N/m^2 in the transverse direction and an equal compressive stress longitudinally. This stress level is sufficient to cause cracking in the transverse direction.

Ultimate Tensile Strength

The ultimate tensile strength of the unidirectional longitudinal sample before cycling was 234×10^6 N/m^2. As was the case in all of the samples, a large drop in the ultimate tensile strength was noted after ten cycles. In this case the value dropped to 120×10^6 N/m^2. Further cycling caused little more damage with the value after 100 cycles being 151×10^6 N/m^2, 1000 cycles 176×10^6 N/m^2 and 5000 cycles 162×10^6 N/m^2.

Table III gives ultimate tensile strengths of the various configurations.

Electron Microscope

Figures 16 through 18 show the fracture surfaces of the unidirectional, $[0/30/60/90/-60/-30]_S$, and the $[[\pm 45_3]_2]_T$ samples.

Figure 16 is the micrograph of the unidirectional sample. It can be seen that the fibers were broken and pulled from the matrix. This is the typical fracture expected in an unidirectional sample. The area shown is one where no delamination appeared.

The second micrograph, Figure 17, is of the $[0/30/60/90/-60/-30]_S$ sample. The first micrograph indicates that there is little delamination even after repeated cycling. The second micrograph is of the boundary area between two layers shown at a magnification of 250X. This is typical boundary area and indicates that there was very good bonding between layers.

Figure 18 is of the $[[\pm 45_3]_2]_T$ sample. It is obvious that there is extensive delamination in this sample. The delamination first started to appear at 100 cycles and became progressively worse as the number of cycles increased. The second photomicrograph shows the complete delamination between two layers after 1000 cycles.

Figure 16. Fracture Surface of Unidirectional Sample 100 Cycles 1000X

100 Cycles 250X

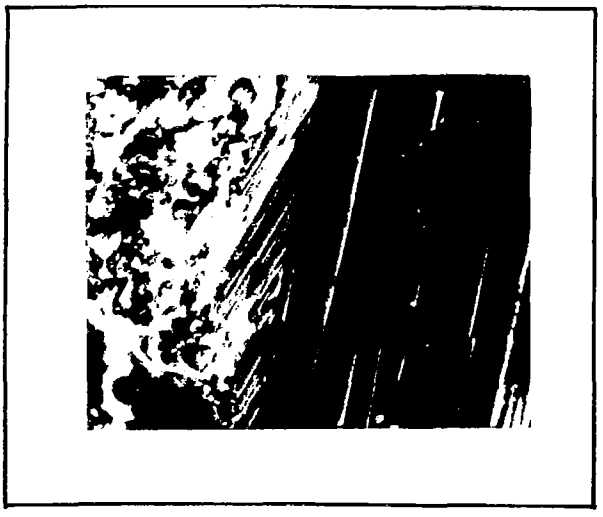

1000 Cycles 250X

Figure 17. Fracture Surface of $[0/30/60/90/-60/-30]_S$ Sample

100 Cycles 60X

1000 Cycles 60X

Figure 18. Fracture Surface of $[[\pm 45_3]_2]_T$ Sample

CONCLUSIONS

Graphite-epoxy laminates were thermally cycled to determine the effects of thermal cycles on tensile and thermal properties of the laminates. Three 12-ply laminate configurations (unidirectional, $[[\pm 45_3]_2]_T$, and $[0/30/60/90/-60/-30]_S$ were subjected to up to 5000 thermal cycles. The cumulative effect of the thermal cycles was determined by destructive inspections (electron microscopy and tests of properties) of samples after progressively larger numbers of cycles. The inspections and tests support the following conclusions:

1. It is possible with careful lamination and curing to obtain graphite-fiber reinforced composites practically free of cracks.
2. Thermal cycling induces cracks through the thickness in the matrix parallel to the fibers in the unidirectional composite.
3. Thermal cycling induces transverse cracking and extensive delamination in the $[[\pm 45_3]_2]_T$ laminated composite.
4. Thermal cycling in the $[0/30/60/90/-60/-30]_S$ sample induces transverse cracks which are continuous across layer interfaces, with occasional localized delamination forming the portions of the crack in adjacent layers.
5. Thermal cycling causes considerable deterioration in the elastic and strength properties of the composites.
6. Thermal cycling causes the thermal expansion coefficient of the cross-plied composites to decrease to approximately one-third of its value. The absolute value of the change, however, is very small.

7. While the structural damage continues to increase as the number of cycles increases, the largest portion of the deterioration of mechanical properties takes place during the first few cycles with subsequent cycles causing only a little further deterioration.
8. In-plane thermal stress in both cross-plied laminates was estimated to be 0.45×10^6 N/m^2/K in the fiber direction and -0.45×10^6 N/m^2/K transverse to the fibers for this graphite-epoxy system.
9. Both cross-plied laminated compostes deteriorated to about the same degree during thermal cycling. The improved strengths expected from the gradual change in orientation in the $[0/30/60/90/-60/-30]_s$ composite was apparently countered by the relative ease of crack propagation.

REFERENCES

1. Handbook of Fiberglass and Advanced Plastic Composites. Edited by George Lubin VanNostrand. Reinhold Company, 1969.

2. Hill, R. (1964). Theory of Mechanical Properties of Fiber Strengthened Materials. Elastic Behavior. Journal of Mechanics and Physics of Solids. Volume 12.

3. Rosen, B. W. (1973). Composite Materials and the Designer Article 3. Stiffness of Fiber Composite Materials. Composites.

4. Ashton, J. E., J. C. Halpin and P. H. Petit (1969). Primer on Composite Material: Analysis. Technomic Publications, Stanford, Connecticut.

5. Spencer, A. J. M. Deformation of Fiber Reinforced Composites. Holden-Day, New York, New York 1963.

6. Fahmy, A. A. and A. N. Ragai (1970). Thermal Expansion of Graphite-Epoxy Composites. Journal of Applied Physics, Volume 41, 5112.

7. Doner, D. R. and R. C. Novak (1969). Structural Behavior of Laminated Graphite Filament Composites. 24th Annual Technical Conference. The Society of the Plastics Industry, Inc.

8. Spain, R. G. (1971). Thermal Microcracking of Carbon/Resin Composites. Composites.